

Rotational evolution of young pulsars due to superfluid decoupling

Wynn C. G. Ho* & Nils Andersson*

Pulsars are rotating neutron stars that are seen to slow down, and the spin-down rate is thought to be due to magnetic dipole radiation^{1,2}. This leads to a prediction for the braking index n , which is a combination of the spin period and its first and second time derivatives. However, all observed values³ of n are below the predicted value of 3. Here we provide a simple model that can explain the rotational evolution of young pulsars, including the $n = 2.51$ of the 958-year-old pulsar in the Crab nebula⁴. The model is based on a decrease in the effective moment of inertia due to an increase in the fraction of the stellar core that becomes superfluid as the star cools through neutrino emission. The results suggest that future large radio monitoring campaigns of pulsars will yield measurements of the neutron star mass, nuclear equation of state, and superfluid properties.

The core of a neutron star has densities near and above nuclear saturation and extends to 90% of the radius of the star; the remaining kilometre or so is the stellar crust. The core is composed of degenerate matter, mostly neutrons and a small fraction of protons and electrons (and possibly exotica, such as hyperons and deconfined quarks, which we do not consider here). Immediately after neutron star formation, this matter is in a normal state due to the high temperatures reached in stellar core collapse. However, neutron stars cool rapidly through the emission of neutrinos, and when the temperature drops below the (density-dependent) critical temperature for Cooper pairing, neutrons and protons form a superfluid and superconductor, respectively^{5,6}. Superfluid neutrons rotate by forming quantized vortices, and the spatial distribution of these vortices determines the rotation rate of the superfluid core; for example, vortices migrate away from the stellar axis of rotation when the superfluid angular velocity Ω_{sf} decreases whereas Ω_{sf} cannot change if the vortices are fixed in location, that is, when they are pinned. Meanwhile, normal matter (for example, in the crust) rotates at an angular velocity Ω that decreases as a result of energy loss from the stellar surface due to magnetic dipole radiation, that is, $dE/dt = -\beta\Omega^4$, where $\beta \approx B^2 R^6 / 6c^3$ and B and R are the neutron star magnetic field and radius, respectively^{1,2}.

A rapid decline in surface temperature was recently detected in the 330-year-old neutron star in the Cassiopeia A supernova remnant^{7,8}. The observed cooling can be understood as being caused by the recent onset of neutron superfluidity in the core of the star, combined with a much earlier onset of proton superconductivity^{8,9}. This has provided the first direct constraints on core superfluid and superconducting properties from neutron star observations. These new results motivate studies of possible implications. Here we explore the rotational evolution of young pulsars using the newly constrained superfluid properties and assuming this superfluid core is allowed to decouple (as discussed below). We use simulations¹⁰ of the cooling of a neutron star to deter-

mine the fraction of the neutron star core that is superfluid as a function of time; this allows us to track the normal and superfluid components of the moment of inertia as the star ages (see Supplementary Fig. S1).

We consider a simple phenomenological model for the rotational evolution of the normal and superfluid components of the star:

$$\frac{d}{dt}(I\Omega) = -\beta\Omega^3 - N_{\text{pin}} - N_{\text{mf}} \quad (1)$$

$$\frac{d}{dt}(I_{\text{sf}}\Omega_{\text{sf}}) = N_{\text{pin}} + N_{\text{mf}}, \quad (2)$$

where I and I_{sf} are the moments of inertia of the normal and superfluid components, respectively, (and $I + I_{\text{sf}} = \text{constant}$) and N_{pin} and N_{mf} are torques associated with vortex pinning¹¹ and dissipative mutual friction¹², respectively. Note that it is the rotation of the normal component Ω that is observed in pulsars. There are three simple limits that we can consider. The first is that friction acts on a much shorter timescale than the spin-down timescale¹²; this is the conventional view of rotational evolution, which leads to Ω_{sf} closely tracking Ω and a braking index $n = 3$ (where $n \equiv \Omega \dot{\Omega} / \dot{\Omega}^2$ and \dot{x} and \ddot{x} are first and second, respectively, time derivatives of the parameter x), at odds with all measured values³. The second limit is when there is no pinning or friction; we find that this leads to $n > 3$. The final case, which we consider in detail here, is when pinning causes $\dot{\Omega}_{\text{sf}} \approx 0$. The evolution equations (1) and (2) can then be combined to give

$$\frac{d\Omega}{dt} = (\Omega_{\text{sf}} - \Omega) \frac{1}{I} \frac{dI}{dt} - \beta \frac{\Omega^3}{I}. \quad (3)$$

The spin lag, $\Omega_{\text{sf}} - \Omega$, is the difference in rotational velocity between the superfluid and normal components. Some examples of decoupled spin evolution are shown in Fig. 1.

Conventional pulsar spin evolution only accounts for the second term on the right-hand side of equation (3), with constant B and I . In this case, pulsars born at a particular spin period ($P = 2\pi/\Omega$) evolve by moving along lines of constant^{13,14} B , and the characteristic age τ_c ($\equiv P/2\dot{P}$) is an estimate of the true age of the pulsar. However, this again suggests that the conventional picture is incomplete: in cases where an independent age can be estimated (for example, from studying the expansion of an associated supernova remnant), the result is often quite different from the characteristic age; this can be seen in Table 1. When superfluid decoupling is taken into account, spin evolution is similar to the conventional course, except now the moment of inertia decreases over time. If the spin lag remains small (for example, as a result of an angular momentum sink acting on the superfluid), only a small deviation (from evolution along a constant B track) is seen at intermediate and late times (after $\sim 1000 - 2000$ yr). Note that we are considering intermediate times ($\sim 10^3 - 10^5$ yr) in the life of a neutron star, in between the short timescale for glitch recurrence¹⁵ (~ 1 yr) and the long timescales for magnetic field diffusion^{13,14} and cooling¹⁶⁻¹⁸ ($\sim 10^5 - 10^6$ yr). On the other hand, if the spin lag is allowed to become large (for example, owing to strong vortex pinning), then we

Received 21 May 2012; accepted 15 August 2012; published online 30 September 2012

School of Mathematics, University of Southampton, Southampton, SO17 1BJ, UK.
*email: wynrho@slac.stanford.edu; n.a.andersson@soton.ac.uk

see that a decreasing I can mimic a strongly increasing magnetic field, leading to pulsars evolving in the way suggested³ for PSR J1734–3333 with $n < 3$. A further departure from the conventional picture is that the characteristic age is not an accurate indication of the true age of a pulsar at early times.

Not only are the spin period P and first time derivative of the period \dot{P} observable quantities, in some cases the second time derivative \ddot{P} can be measured. This provides another test for our model. Table 1 gives data on eight systems where the braking index n , which is proportional to \ddot{P} , has been measured, whereas our model predicts the braking index to be [see equation (3)]

$$n = 3 - \frac{2\dot{I}}{I} \frac{\Omega}{\dot{\Omega}} - \left(\frac{3\dot{I}}{I} \frac{\Omega}{\dot{\Omega}} - \frac{\ddot{I}}{I} \frac{\Omega^2}{\dot{\Omega}^2} \right) \left(\frac{\Omega_{\text{sf}}}{\Omega} - 1 \right) = 3 - 4\tau_c \left| \frac{\dot{I}}{I} \right|, \quad (4)$$

where the second equality is obtained when $\Omega_{\text{sf}} - \Omega \ll \Omega$.

As τ_c and n are observable quantities (related simply to P , \dot{P} , and \ddot{P}) for a given pulsar, we can compare our predictions to the pulsars in Table 1; this is shown in Fig. 2. For the Crab pulsar (the only one with a known age), we infer a relatively high mass of $\approx 1.8 M_{\text{Sun}}$ (for the particular equation of state and superfluid properties we consider; see Supplementary Information). Furthermore, we can use the mass determination to estimate the initial period and magnetic field of the pulsar, and we find an initial period ~ 0.02 s and $B \sim 4 \times 10^{12}$ G.

The fact that our simple model is able to explain the observed pulsar properties demonstrates the merits of the notion of decoupled spin-evolution due to the onset of core superfluidity. However, key questions remain to be understood. The main assumption in our model is that core superfluid neutrons are allowed to decouple and pin. Core pinning is thought to be the result of the interaction between superfluid vortices and fluxtubes in the proton superconductor¹¹. Whether this mechanism can be strong enough to act in the way assumed in our analysis is not clear at this time. Theoretical work is also required to determine whether the spin-lag $\Omega_{\text{sf}} - \Omega$ can be kept small during the evolution by an (at this time) unspecified angular momentum sink. From an observational point-of-view, discovery and long-term monitoring of a large number of systems by radio telescopes such as LOFAR and SKA will allow accurate timing of many young pulsars in the future. Taking these pulsars as an ensemble, we can constrain the nuclear equation of state and superfluid properties (because these determine the evolution of the moment of inertia), analogous to what is done in studies of neutron star thermal evolution. Knowledge of these properties can then be used to infer the mass of individual pulsars. Finally, radio timing measurements may be able to constrain neutron star thermal evolution, independently of measurements at X-ray energies.

Note added in proof. After completion of this work, we became aware of the independent development of a similar mechanism for variation of the pulsar-braking index that was presented by E. Kantor at two conferences in 2011 (<http://go.nature.com/sxaWeN>; <http://go.nature.com/veAOT1>).

- Pacini, F. Rotating neutron stars, pulsars and supernova remnants. *Nature* **219**, 145–146 (1968).
- Gunn, J. E. & Ostriker, J. P. Magnetic dipole radiation from pulsars. *Nature* **221**, 454–456 (1969).
- Espinoza, C. M., Lyne, A. G., Kramer, M., Manchester, R. N., & Kaspi, V. M. The braking index of PSR J1734–3333 and the magnetar population. *Astrophys. J.* **741**, L13–16 (2011).
- Lyne, A. G., Pritchard, R. S., & Graham-Smith, F. 23 years of Crab pulsar rotational history. *Mon. Not. R. Astron. Soc.* **265**, 1003–1012 (1993).
- Migdal, A. B. Superfluidity and the moments of inertia of nuclei. *Sov. Phys. JETP* **10**, 176–185 (1960).
- Baym, G., Pethick, C., & Pines, D. Superfluidity in neutron stars. *Nature* **224**, 673–674 (1969).
- Heinke, C. O. & Ho, W. C. G. Direct observation of the cooling of the Cassiopeia A neutron star. *Astrophys. J.* **719**, L167–L171 (2010).

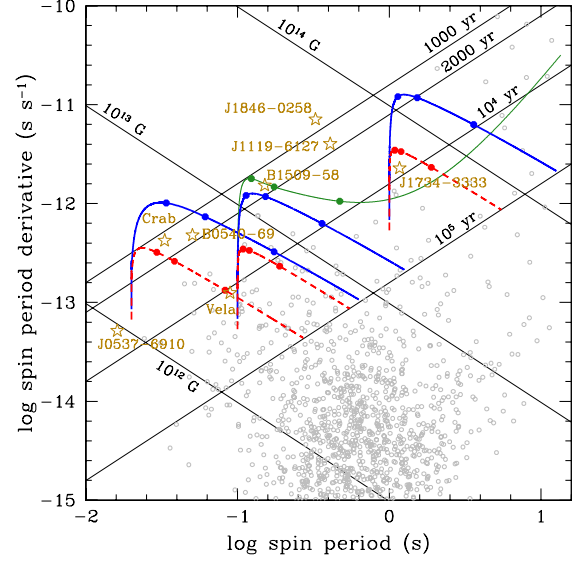


Figure 1 | Pulsar spin period versus spin period derivative. The open circles are observed values taken from the ATNF Pulsar Catalogue¹⁹. The stars denote pulsars with a measured braking index (see Table 1). The thin diagonal lines denote characteristic age ($= P/2\dot{P}$) and inferred magnetic field [$= 3.2 \times 10^{19} \text{ G} (P\dot{P})^{-1/2}$]. The curves are spin evolution tracks for pulsars with mass $1.8 M_{\text{Sun}}$ (red, dashed) and $1.4 M_{\text{Sun}}$ (blue, solid), where the spin lag is maintained at $\Omega_{\text{sf}}/\Omega - 1 \leq 10^{-6}$ (by an additional angular momentum sink); the filled circles denote the evolution at ages 1000, 2000, and 10^4 yr. Also shown (green, thin solid) is the evolution of a pulsar where the spin lag is allowed to grow. From left to right, the initial spin period and magnetic field (P , B) are taken to be (0.02 s, 5×10^{12} G), (0.1 s, 10^{13} G), and (1 s, 10^{14} G). These examples demonstrate that the model can explain the observed pulsar population.

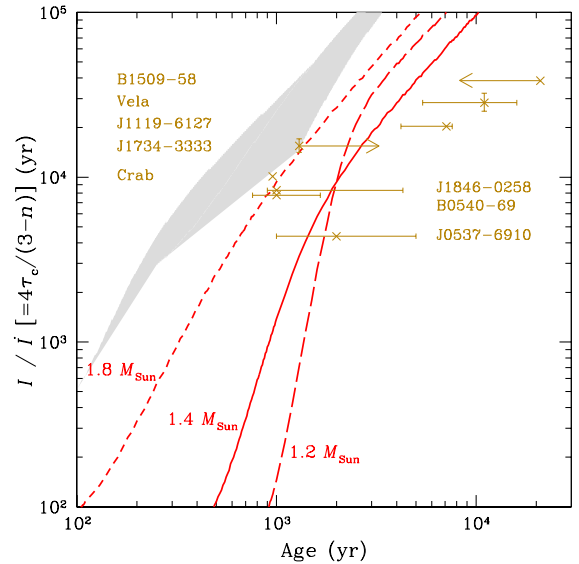


Figure 2 | Constraining neutron star properties. The crosses denote pulsars with a measured braking index; horizontal bars and arrows indicate uncertainties or limits on their true age, and vertical bars are shown for pulsars with larger braking index uncertainty. The curves show the evolution of the effective moment of inertia for pulsars with mass $1.8 M_{\text{Sun}}$ (short-dashed), $1.4 M_{\text{Sun}}$ (solid), and $1.2 M_{\text{Sun}}$ (long-dashed), assuming a particular stellar and superfluid model⁹, and the shaded region represents an alternative model⁸; both sets of superfluid parameters fit the rapid cooling seen in the Cassiopeia A neutron star (see Supplementary Information) and provide examples of the effect of different $|I/\dot{I}|$ models [see equation (4)]. These moment of inertia evolution curves are analogous to the thermal cooling curves^{16–18} used to determine properties of neutron stars.

Pulsar name	Supernova remnant	Period (s)	Period derivative ($s s^{-1}$)	Characteristic age τ_c (yr)	Braking index n	Age (yr)
B0531+21	Crab	0.0331	4.23×10^{-13}	1240	2.51(1) (ref. 4)	958
J0537–6910	N157B	0.0161	5.18×10^{-14}	4930	–1.5(1) (ref. 20)	2000^{+3000}_{-1000} (ref. 21)
B0540–69	0540–69.3	0.0505	4.79×10^{-13}	1670	2.140(9) (ref. 22)	1000^{+660}_{-240} (ref. 23)
B0833–45	Vela	0.0893	1.25×10^{-13}	11300	1.4(2) (ref. 24)	11000^{+5000}_{-5600} (ref. 25)
J1119–6127	G292.2–0.5	0.408	4.02×10^{-12}	1610	2.684(2) (ref. 26)	7100^{+500}_{-2900} (ref. 27)
B1509–58	G320.4–1.2	0.151	1.54×10^{-12}	1550	2.839(3) (ref. 22)	< 21000 (ref. 28)
J1846–0258	Kesteven 75	0.325	7.08×10^{-12}	729	2.65(1) (ref. 22)	1000^{+3300}_{-100} (ref. 29)
J1734–3333	G354.8–0.8	1.17	2.28×10^{-12}	8120	0.9(2) (ref. 3)	> 1300

Table 1 | Pulsars with observed braking index. The periods and period derivatives are taken from ref. 19. The numbers in parentheses show braking index uncertainty in the last digit. For J1734–3333, we give a lower limit of the age, which we estimate by considering the supernova remnant size (21 parsecs; ref. 30) and remnant expansion velocity v_{SNR} , to obtain an age $\sim 2000 \text{ yr}$ ($10^4 \text{ km s}^{-1}/v_{\text{SNR}}$); and considering the pulsar’s distance away from the centre of the supernova remnant (46 parsecs; ref. 30) and pulsar space velocity v_{pulsar} , to obtain an age $\sim 23000 \text{ yr}$ ($2000 \text{ km s}^{-1}/v_{\text{pulsar}}$).

8. Shternin, P. S., Yakovlev, D. G., Heinke, C. O., Ho, W. C. G. & Patnaude, D. J. Cooling neutron star in the Cassiopeia A supernova remnant: Evidence for superfluidity in the core. *Mon. Not. R. Astron. Soc.* **412**, L108–L112 (2011).
9. Page, D., Prakash, M., Lattimer, J. M., & Steiner, A. W. Rapid cooling of the neutron star in Cassiopeia A triggered by neutron superfluidity in dense matter. *Phys. Rev. Lett.* **106**, 081101–1–4 (2011).
10. Ho, W. C. G., Glampedakis, K., & Andersson, N. Magnetars: super(ficially) hot and super(fluid) cool. *Mon. Not. R. Astron. Soc.* **422**, 2632–2641 (2012).
11. Link, B. Constraining hadronic superfluidity with neutron star precession. *Phys. Rev. Lett.* **91**, 101101–1–4 (2003).
12. Alpar, M. A., Langer, S. A., & Sauls, J. A. Rapid postglitch spin-up of the superfluid core in pulsars. *Astrophys. J.* **282**, 533–541 (1984).
13. Goldreich, P. & Reisenegger, A. Magnetic field decay in isolated neutron stars. *Astrophys. J.* **395**, 250–258 (1992).
14. Glampedakis, K., Jones, D. I., & Samuelsson, L. Ambipolar diffusion in superfluid neutron stars. *Mon. Not. R. Astron. Soc.* **413**, 2021–2030 (2012).
15. Espinoza, C. M., Lyne, A. G., Stappers, B. W., & Kramer, M. A study of 315 glitches in the rotation of 102 pulsars. *Mon. Not. R. Astron. Soc.* **414**, 1679–1704 (2011).
16. Tsuruta, S. Thermal properties and detectability of neutron stars. II. Thermal evolution of rotation-powered neutron stars. *Phys. Rep.* **292**, 1–130 (1998).
17. Yakovlev, D. G. & Pethick, C. J. Neutron star cooling. *Annu. Rev. Astron. Astrophys.* **42**, 169–210 (2004).
18. Page, D., Geppert, U., & Weber, F. The cooling of compact stars. *Nucl. Phys. A* **777**, 497–530 (2006).
19. Manchester, R. N., Hobbs, G. B., Teoh, A., & Hobbs, M. The Australia Telescope National Facility Pulsar Catalogue. *Astron. J.* **129**, 1993–2006 (2005).
20. Middleditch, J., Marshall, F. E., Wang, Q. D., Gotthelf, E. V. & Zhang, W. Predicting the starquakes in PSR J0537–6910. *Astrophys. J.* **652**, 1531–1546 (2006).
21. Chen, Y., Wang, Q. D., Gotthelf, E. V., Jiang, B., Chu, Y.-H., & Gruendl, R. Chandra ACIS spectroscopy of N157B: a young composite supernova remnant in a superbubble. *Astrophys. J.* **651**, 237–249 (2006).
22. Livingstone, M. A., Kaspi, V. M., Gavriil, F. P., Manchester, R. N., Gotthelf, E. V. G., & Kuiper, L. New phase-coherent measurements of pulsar braking indices. *Astrophys. Space Sci.* **308**, 317–323 (2007).
23. Park, S., Hughes, J. P., Slane, P. O., Mori, K., & Burrows, D. N. A deep Chandra observation of the oxygen-rich supernova remnant 0540–69.3 in the Large Magellanic Cloud. *Astrophys. J.* **710**, 948–957 (2010).
24. Lyne, A. G., Pritchard, R. S., Graham-Smith, F., & Camilo, F. Very low braking index for the Vela pulsar. *Nature* **381**, 497–498 (1996).
25. Page, D., Lattimer, J. M., Prakash, M., & Steiner, A. W. Neutrino emission from Cooper pairs and minimal cooling of neutron stars. *Astrophys. J.* **707**, 1131–1140 (2009).
26. Weltevrede, P., Johnston, S., & Espinoza, C. M. The glitch-induced identity changes of PSR J1119–6127. *Mon. Not. R. Astron. Soc.* **411**, 1917–1934 (2011).
27. Kumar, H. S., Safi-Harb, S., & Gonzalez, M. E. Chandra and XMM-Newton studies of the supernova remnant G292.2–0.5 associated with the pulsar J1119–6127. *Astrophys. J.* **754**, 96–1–14 (2012).
28. Gaensler, B. M., Brazier, K. T. S., Manchester, R. N., Johnston, S., & Green, A. J. SNR G320.4–01.2 and PSR B1509–58: new radio observations of a complex interacting system. *Mon. Not. R. Astron. Soc.* **305**, 724–736 (1999).
29. Blanton, E. L. & Helfand, D. J. ASCA observations of the composite supernova remnant G29.7–0.3. *Astrophys. J.* **470**, 961–966 (1996).
30. Manchester, R. N. et al. in *Neutron Stars in Supernova Remnants* (eds Slane, P. O. & Gaensler, B. M.) 31 (ASP Conf. Ser. 271, Astronomical Society of the Pacific, 2002).

Acknowledgements

W.C.G.H. thanks D. Yakovlev for providing equation of state tables. W.C.G.H. appreciates the use of the computer facilities at the Kavli Institute for Particle Astrophysics and Cosmology. W.C.G.H. and N.A. acknowledge support from the Science and Technology Facilities Council (STFC) in the United Kingdom.

Author contributions

W.C.G.H. contributed to developing the model, performed the calculations, and

wrote the manuscript. N.A. contributed to developing the model and writing the manuscript.

Additional information

Supplementary information is available in the online version of the paper. Reprints and permissions information is available online at www.nature.com/reprints. Correspondence and requests for materials should be addressed to W.C.G.H. or N.A.

Competing financial interests

The authors declare no competing financial interests.

Supplementary Information

Neutron star cooling and moment of inertia evolution

Neutron stars begin their lives very hot (with temperatures $T > 10^{11}$ K) but cool rapidly through the emission of neutrinos. Neutrino emission processes depend on uncertain physics at the supra-nuclear densities ($\rho > 2.8 \times 10^{14}$ g cm $^{-3}$) of the neutron star core^{16–18}. The recent observation of rapid cooling^{7,8} of the neutron star in the Cassiopeia A supernova remnant provides the first constraints on the (density-dependent) critical temperatures for the onset of superfluidity of core protons T_{cp} (in the singlet state) and neutrons T_{cnt} (in the triplet state), that is, $T_{cp} \sim (2-3) \times 10^9$ K and a maximum $T_{cnt} \approx 5 \times 10^8$ K for a superfluid neutron model at relatively shallow densities⁹ or a maximum $T_{cnt} \approx (7-9) \times 10^8$ K for a superfluid neutron model at deep densities⁸.

We calculate the thermal evolution of neutron stars by solving the relativistic equations of energy balance and heat flux. We use a stellar model based on the APR equation of state and consider either the shallow or deep model for triplet neutron pairing in the core¹⁰. Note that we improve upon the calculations of ref. 10 by using more accurate ion and electron heat capacities³¹. Due to high thermal conductivity, neutron stars after $\sim 10 - 100$ yr are essentially isothermal^{32–34}; the exact time is unimportant for our work since the youngest neutron star we consider has an age ≈ 1000 yr (see Table 1). The evolution of the (gravitationally redshifted) surface temperature for models with the shallow neutron superfluid and an unmagnetized iron envelope is shown in Fig. S1. Enhanced neutrino emission due to Cooper pairing of neutrons begins to occur at the onset of superfluidity in the core. At an age of a few hundred to one thousand years, large portions of the (predominantly neutron) stellar core become superfluid, and rapid cooling occurs.

We calculate the moment of inertia of the normal and superfluid components by³⁵

$$I = \frac{8\pi}{3} \int_0^R (\rho + P/c^2) \Lambda r^4 dr, \quad (5)$$

where P is the local pressure, $\Lambda = (1 - 2Gm/c^2r)^{-1}$, and m is the mass enclosed within r . Note that we neglect for simplicity a term that approximately accounts for relativistic frame-dragging³⁵, which would only change I by $< 10\%$. Fig. S1 shows the evolution of the normal component of I .

In order to facilitate numerical calculations of $\dot{I}(t)$ and $\ddot{I}(t)$, we fit $I(t)$ with the following function

$$\log I = a_3 \tanh[a_2(\log t - a_1)] + (\log t - b_1)^{b_2} + c_1, \quad (6)$$

where the fit parameters $a_1, a_2, a_3, b_1, b_2, c_1$ are given in Table S1. A comparison of the approximate fit to the exact result is shown in Fig. S1. Note that the largest deviations occur briefly at (early) times that are not of current relevance.

We note that we only consider a single model for the nuclear equation of state and two models for the neutron superfluid gap. Exploration of a larger range of models (in order to obtain, for example, error bars on neutron star mass) is required and the subject of future work.

Neutron star mass	a_1	a_2	a_3	b_1	b_2	c_1
$1.2 M_{\text{Sun}}$	2.90	7.4	-1.5	0.10	-1.0	45.24
$1.4 M_{\text{Sun}}$	2.59	4.6	-1.2	0.95	-1.2	44.97
$1.8 M_{\text{Sun}}$	1.98	2.6	-0.31	0	-1.6	44.945

Table S1 | Fit parameters for moment of inertia evolution.

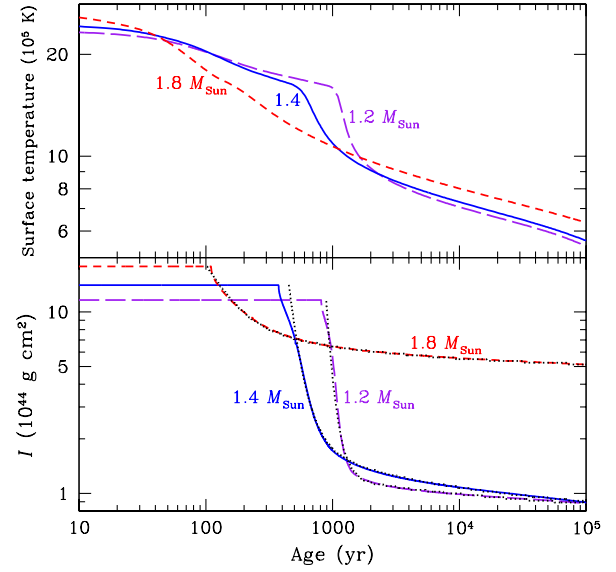


Figure S1 | Thermal and moment of inertia evolution of neutron stars. The curves show the evolution of the surface temperature (top) and moment of inertia (bottom) for neutron stars with mass $1.8 M_{\text{Sun}}$ (red, short-dashed), $1.4 M_{\text{Sun}}$ (blue, solid), and $1.2 M_{\text{Sun}}$ (purple, long-dashed). The dotted curves show analytic fits using equation (6).

31. Potekhin, A.Y. & Chabrier, G. Thermodynamic functions of dense plasmas: Analytic approximations for astrophysical applications. *Contrib. Plasma Phys.* **50**, 82–87 (2010).
32. Lattimer, J. M., van Riper, K. A., Prakash, M., & Prakash, M. Rapid cooling and the structure of neutron stars. *Astrophys. J.* **425**, 802–813 (1994).
33. Gnedin, O. Y., Yakovlev, D. G., & Potekhin, A. Y. Thermal relaxation in young neutron stars. *Mon. Not. R. Astron. Soc.* **324**, 725–736 (2001).
34. Yakovlev, D. G., Ho, W. C. G., Shternin, P. S., Heinke, C. O., & Potekhin, A. Y. Cooling rates of neutron stars and the young neutron star in the Cassiopeia A supernova remnant. *Mon. Not. R. Astron. Soc.* **411**, 1977–1988 (2011).
35. Ravenhall, D. G. & Pethick, C. J. Neutron star moments of inertia. *Astrophys. J.* **424**, 846–851 (1994).